A&A 507, 855–860 (2009)
DOI: 10.1051/0004-6361/200912825

Astronomy & Astrophysics

The interaction of an O star wind with a Herbig-Haro jet

A. Esquivel[1], A. C. Raga[1], J. Cantó[2], and A. Rodríguez-González[1]

[1] Instituto de Ciencias Nucleares, Universidad Nacional Autónoma de México, Ap. Postal 70-543, 04510 D.F., México
e-mail: [esquivel;raga]@nucleares.unam.mx
[2] Instituto de Astronomía, Universidad Nacional Autónoma de México, Ap. Postal 70-468, 04510 D.F., México

Received 3 July 2009 / Accepted 4 September 2009

ABSTRACT

Context. Herbig-Haro jets ejected from young, low mass stars in the proximity of O/B stars will interact with the more or less isotropic winds from the more massive stars. An example of this are the jets from the stars within the proplyds near θ-Orionis.
Aims. In this paper, we consider the interaction of an externally photoionized HH jet with an isotropic wind ejected from the ionizing photon source. We study this problem through numerical simulations, allowing us to obtain predictions of the detailed structure of the flow and predictions of Hα intensity maps. This is a natural extension of a previously developed analytic model for the interaction between a jet and an isotropic stellar wind.
Methods. We present 3D simulations of a bipolar HH jet interacting with an isotropic wind from a massive star, assuming that the radiation from the star photoionizes all of the flow. We describe different possible flow configurations, exploring a limited set of jet and stellar wind parameters and orientations of the jet/counterjet ejection. We have computed 6 models, two of which also include a time-variability in the jet velocity.
Results. We compare the locus of the computed jet/counterjet systems with the analytic model, and find very good agreement except for cases in which the direction of the jet (or the counterjet) approaches the direction to the wind source (i.e., the O star). For the models with variable ejection velocities, we find that the internal working surfaces follow straighter trajectories (and the inter-working surface segments more curved trajectories) than the equivalent steady jet model.

Key words. ISM: kinematics and dynamics – ISM: jets and outflows – ISM: Herbig-Haro objects – stars: winds, outflows

1. Introduction

In a recent paper, Raga et al. (2009a) presented an analytic model for the interaction of a steady Herbig-Haro (HH) jet (from a young, low mass star) with an isotropic wind (from a more massive, nearby young star). The isotropic wind source could be a Herbig Ae/Be star, or an O/B star.

This model was an extension of the jet/sidewind analytic model of Cantó & Raga (1995), incorporating the divergence of the wind which impinges on the HH jet. The HH jet/plane-parallel sidewind scenario has also been studied with 3D gas-dynamic simulations (Lim & Raga 1998; Masciadri & Raga 2001; Kajdič & Raga 2007; Ciardi et al. 2008), and successful comparisons with the analytic model of Cantó & Raga (1995) have been made.

In this paper, we present 3D gas-dynamic simulations of the interaction between an isotropic wind from an O star and a HH jet. We present models of jets with a steady ejection velocity, and also with a sinusoidally varying velocity. We explore the effects of different parameter combinations, including the direction of ejection (with respect to the direction to the wind source) of the jet/counterjet systems. Comparisons with the analytic model of Raga et al. (2009a) are carried out.

Our simulations allow us to make predictions of observable parameters. In particular, we present Hα emission line maps, which in principle can be compared with images of candidate systems.

It is actually not clear to which objects our O star wind/HH jet model could be applied. Possible candidates are the jets ejected from the proplyds located within or in the proximity of the θ^1-Ori Trapezium in M42, such as HH 508, HH 514 and the jet/counterjet system that is possibly being powered by the 167–317 (LV2) proplyd (see Bally et al. 2000). These systems are likely to be embedded within the stellar winds of the θ^1-Ori stars, and therefore represent possible jet/wind interaction systems. Unfortunately, these jets are barely detected in HST images, with identified lengths of $\sim 1''$. Therefore, it is not possible to say whether or not they curve away from the stellar wind sources, as expected.

The much larger scale, curved jets seen at larger distances from θ^1-Ori (see Bally & Reipurth 2001; Bally et al. 2006) are not immersed in the wind from the θ^1-Ori stars, and are interacting with the expanding M42 nebula. Therefore, they are not candidates for modeling with the simulations described in the present paper.

This lack of a clear astrophysical counterpart for the simulations of the present paper is of course somewhat problematic. At the end of the paper, we discuss what kind of observations are necessary in order to solve this problem.

The paper is organized as follows. The analytic model of Raga et al. (2009a) is summarized in Sect. 2. The setup of the numerical simulations is described in Sect. 3. A description of the results and comparisons with the analytic model of Raga et al. (2009a) are presented in Sect. 4. Predictions of observable quantities are discussed in Sects. 5 and 6. Finally, the results are summarized in Sect. 7.

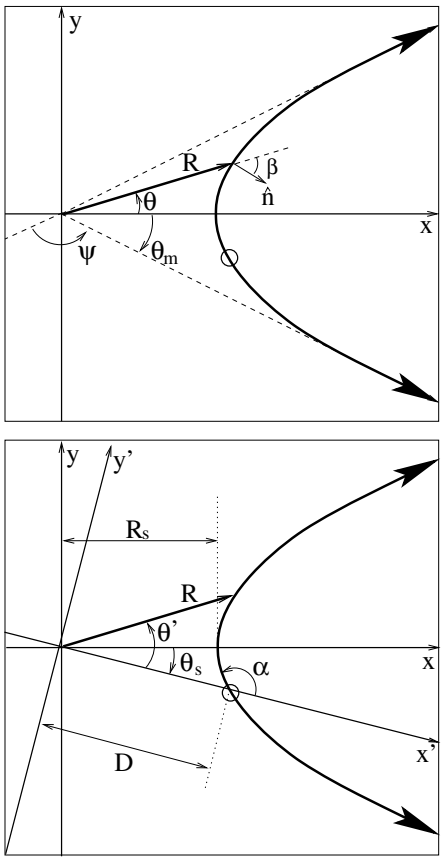

Fig. 1. (Reproduced with permission from Raga et al. 2009a) Schematic of the coordinate system(s) of the analytic model of the interaction of a HH jet and a star. *Top frame*: the star is placed at the origin of the *xy*-coordinate system, and the "stagnation point" (point of maximum approach between the star and the jet/counterjet path) is aligned with the x-axis. The jet/counterjet locus is described by $R(\theta)$, where θ is the angle measured counterclockwise form the x-axis. Maximum deflection is achieved at an angle θ_m, when the direction of the jet/counterjet is radial with respect to the star and $R(\pm\theta_m) \to \infty$. The total deflection of the jet is $\Psi = \pi - 2\theta_m$. *Bottom frame*: two frames of reference with their origin centered at the wind source. The *xy*-system coincides with that of the *top panel*, the $x'y'$-system is rotated so that the abscissa is in the line that joins the jet source with the wind source. The jet source is placed at a distance D and ejects material at angle α, measured counterclockwise from the x'-axis. The angle subtended by the jet source, the wind source, and the stagnation point is θ_s (θ_s is always positive).

2. The analytic model

The shape of a jet/counterjet system, immersed in an external wind, can be obtained balancing the ram pressure of the wind (impinging on the side of the jet) with the centrifugal pressure of the material along the curved jet path. Cantó & Raga (1995) modeled the interaction of a plane-parallel wind with a jet, assuming that the cross section of the jet is that of an isothermal "plasmon". Following the same idea, but adopting a more appropriate coordinate system for the model, the interaction of a jet/counterjet system with an isotropic wind was presented in Raga et al. (2009a).

A schematic of the geometry of the problem is shown in Fig. 1.

Balancing the ram pressure that the stellar wind exerts on the side of the jet, with the centrifugal force of the jet following a curved trajectory such that its cross section preserves an isothermal plasmon shape, we obtain the differential equation

$$(\epsilon + 1)R^2 + (2\epsilon + 1)R'^2 - \epsilon R R'' = 0\,, \tag{1}$$

where the dimensionless parameter ϵ is given by

$$\epsilon = 2\left(\frac{\dot{M}_j v_j}{\dot{M}_w v_w}\right)^{1/2} \frac{v_j}{c_j}\,. \tag{2}$$

This equation can be integrated two times (with the appropriate boundary conditions) to obtain

$$R = \frac{R_s}{\cos^\lambda(\theta/\lambda)}\,; \quad \lambda \equiv \epsilon/(1+\epsilon)\,, \tag{3}$$

where θ is the angle measured (counterclockwise) from the line that joins the wind source and the stagnation stand-off distance $R_s = R(0)$. The maximum deflection is obtained when $R(\theta_m) \to \infty$, which happens for

$$\theta_m = \lambda\frac{\pi}{2}\,, \tag{4}$$

thus, the total deflection angle is

$$\Psi = \pi - 2\theta_m = \frac{\pi}{1+\epsilon}\,. \tag{5}$$

The solution is symmetrical with respect to the x-axis (the line that passes through the star and the stagnation point), and for a given stagnation distance R_s, the ϵ parameter controls the total deflection angle. For small values of ϵ the momentum in the wind is larger, therefore the jet/counterjet locus is more curved.

Alternatively, one could write the solution in the primed reference system (the abscissa aligned with the wind and jet sources, see Fig. 1). To do this one has to note that

$$\tan\left(\frac{\pi}{2} - \alpha\right) = \left(\frac{R'}{R}\right)_{\theta_s}\,, \tag{6}$$

and use the solution in Eq. (3) to find a relation between the angles θ_s and α:

$$\theta_s = \lambda\left(\alpha - \frac{\pi}{2}\right). \tag{7}$$

This can be used to obtain R_s in units of D:

$$R_s = D\,[\sin\alpha]^\lambda\,. \tag{8}$$

Finally, combining Eqs. (7)–(8) with $\theta = \theta' - \theta_s$ one obtains

$$R(\theta') = D\left[\frac{\sin\alpha}{\sin(\alpha - \theta'/\lambda)}\right]^\lambda. \tag{9}$$

This expression is useful to constrain ϵ and R_s from observations, in which D and α are more easily measured. A more detailed discussion of this analytic model is given by Raga et al. (2009a)

3. The numerical simulations

3.1. The code

We used a 3D hydrodynamical code to compute 6 different models of the interaction of a massive star with a HH jet. The code integrates the gas-dynamic equations on a regular, uniform Cartesian grid, using a second order finite volume method with

Table 1. Model parameters[a]

Model	$v_{j,0}$ [km s^{-1}]	$\dot{M}_w$ [$M_\odot$ yr^{-1}]	x_j [b] [cm]	y_j [c] [cm]	δv [km s^{-1}]	τ_j [yr]	α_y [°]	ϵ
M1	200	4.5×10^{-7}	7×10^{16}	0	0	–	0	3.85
M2	100	10^{-6}	7×10^{16}	0	0	–	0	0.91
M3	100	10^{-6}	7×10^{16}	0	50	10	0	0.91
M4	200	4.5×10^{-7}	7.53×10^{16}	-5.6×10^{16}	0	–	−9.6	3.85
M5	100	10^{-6}	9.54×10^{16}	-6.13×10^{16}	0	–	−35.96	0.91
M6	100	10^{-6}	9.54×10^{16}	-6.13×10^{16}	50	10	−35.96	0.91

[a] In all the models the mass loos rate per side of the jet/counterjet is $\dot{M}_j = 10^{-7}\ M_\odot$ yr^{-1}, and the wind terminal velocity is $v_w = 2\,250$ km s^{-1}; [b,c] measured from the location of the wind source.

HLLC fluxes (Toro et al. 1994), and piecewise linear reconstruction with a *minmod* slope limiter. The code is parallel, with a domain split in blocks arranged in a Cartesian grid, implemented by the Message Passing Interface (MPI) library.

In our simulations H is fully ionized throughout the flow, as a result of the photoionizing radiation from the O star. We do not consider the possibility of an ionization front being trapped within the body of the jet (see Masciadri & Raga 2001). In the energy equation, we include a parametrized cooling function (see Raga et al. 2009b for a detailed description). As we have assumed that the flow is fully photoionized, we have imposed a minimum temperature of 10^4 K, corresponding to the approximate temperature resulting from photoionization equilibrium.

3.2. Numerical setup

We computed 6 models of the interaction of a HH jet with an isotropic wind, in a cubic computational domain with 1.6×10^{17} cm per side, and 256^3 cells, yielding a resolution of 6.25×10^{14} cm^{-1} along the three axes.

A summary of the parameters we used is given in Table 1. The position of the stellar wind source is fixed in all models, centered on the yz-plane, located at 1×10^{16} cm from the left boundary along the x-direction.

In a sphere of radius 5×10^{15} cm centered at this position, we inject an isotropic wind with a temperature of $T_w = 10^5$ K and a terminal velocity v_w. Inside the sphere the density follows an $\propto r^{-2}$ law (r being the spherical radius) scaled so that the mass loss rate is $\dot{M}_w$.

At a position $(x_j, y_j, 0)$ from the wind source, (see Table 1) we place a bipolar cylindrical jet (with 2×10^{15} cm of radius and length), with a top hat profile and a $\dot{M}_j = 10^{-7}\ M_\odot$ yr^{-1} mass loss rate (for each outflow lobe). The jet/counterjet axis is oriented at an angle α_y with respect to the y-axis, and is always perpendicular to the z-axis. The jet material is injected with a temperature $T_j = 10^4$ K, and both the jet and the wind are fully ionized.

In models M1–M3 the jet source is placed at the stagnation point, thus the ejection velocity is perpendicular to the wind at that position. Models M4–M6 are placed along the analytical solution of the path from models M1–M3, respectively, at the appropriate off-axis angle. For models M1, M2, M4, and M5 the jet/counterjet speed is time-independent ($v_j = v_{j,0}$). Models M3 and M6 have the same parameters as M2 and M5, respectively, but have a time-dependent ejection velocity of the form:

$$v_j(t) = v_{j,0} + \delta v_j \sin\left(\frac{2\pi t}{\tau_j}\right). \quad (10)$$

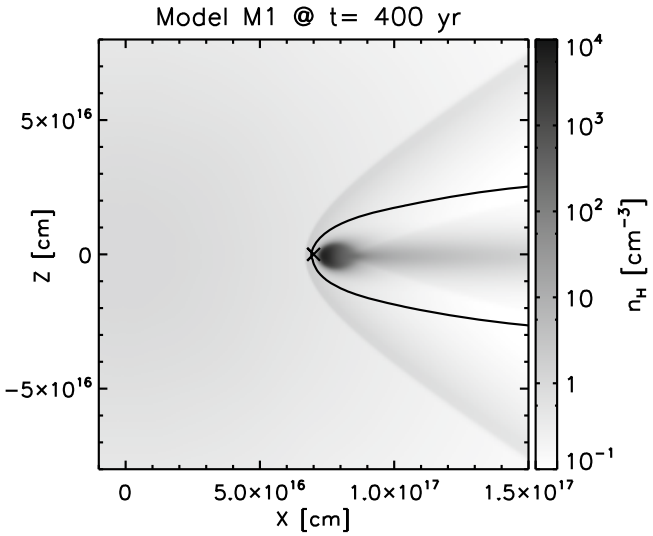

Fig. 2. Cross section of the jet: density stratification in the $y = 6.5\times10^{16}$ cm plane for model M1. The scale is logarithmic, with values indicated by the gray-scale bar (colorbar in the online version) at the right. The cross at the center marks the projected position of the jet source. The solid line shows a contour that separates the wind and jet material (i.e. all the material to the right of this line originated at the jet source, material to the left from the stellar wind source).

4. Results

We let all models evolve until the jet leaves the computational domain, which varies for each model, but is always of ∼500 yr.

As mentioned above, the analytical model considers the motion in the plane defined by the jet/counterjet axis and the wind source, which we have chosen to lie on the xy-plane of our simulations. In Fig. 2 we present a transverse cut (corresponding to the $y = 6.5\times10^{16}$ cm plane) of the density stratification of model M1, after an integration time of 400 yr. From this figure, the plasmon-shaped cross section of the jet is evident. In the figure we marked the position of the jet source, we can see that the densest region (body of the jet) has displaced to the right at this distance. In addition, we have traced the material ejected by the wind and jet sources, with a passive scalar that is proportional to the density but that has opposite sign. The solid line shows the position where the passive scalar changes sign, to the left we have stellar wind material, and jet material to the right.

In Fig. 3 we present cuts of the density stratification on the xy-midplane for all the models after the jet and counterjet have left the grid boundaries. The integration times for each model are indicated in the upper-left hand corner of the panels. Also, for each model, we overlaid the analytical solution of the

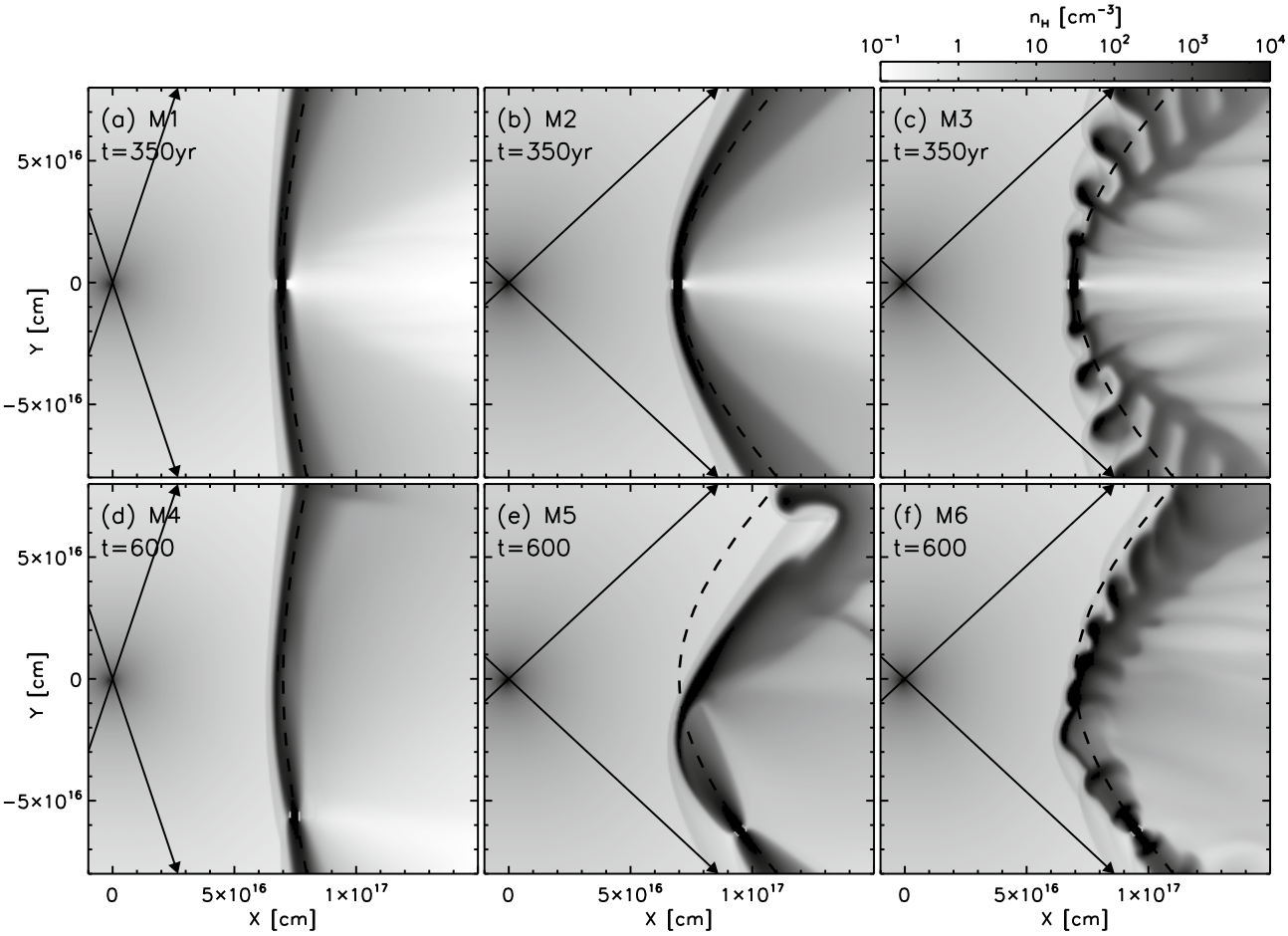

Fig. 3. The path followed by the jet: density cuts in the *xy*-midplane in logarithmic scale, as given by the gray-scale bar (colorbar in the online version) at the *top*, for all models. The model and integration time are indicated in the label at the upper-left corner of each frame. The *dashed*-line shows the analytical solution of Raga et al. (2009a), and the arrows the expected maximum deflection, obtained from the analytical model as well.

jet/counterjet locus (*dashed* curve), and the maximum deflection angle expected, indicated by the arrows in each panel.

We can see from Fig. 3 that the paths described by the jet/counterjet systems in models M1, M2 and M4 agree remarkably well with the predictions from the analytic model (see Sect. 2 and Raga et al. 2009a). These three models have a constant ejection velocity. In M1 and M2 the jet source is placed at the stagnation point (therefore the jet is ejected perpendicularly to the stellar wind). Model M4 has the same parameters as M1, but is placed off the axis formed by the stagnation point and the star, however due to the small ϵ parameter it also makes a large angle with the direction of the wind.

The jet source of model M5, which is otherwise identical to M2, is almost aligned against the wind source. The resulting jet becomes unstable and breaks before reaching the theoretical stagnation point.

For the models with a variable ejection velocity we obtain very similar results. Model M3, (that corresponds to model M2 plus a sinusoidal velocity variation) shows a series of internal working surfaces that open up as they travel away from the jet source. The internal working surfaces are denser, and follow straighter trajectories than the analytical model. At the same time the regions between the successive working surfaces have trajectories that curve more than the analytical model. Model M6, which also has a time-variable ejection velocity, but is closely directed with the direction towards the star (like M5), shows the same trends observed in the other models. As with model M3, the internal working surfaces follow straighter paths than the constant injection counterpart (M5), while the inter-knot regions are swept more easily by the stellar wind, and therefore are more curved. However, as observed as well in model M5, the jet is considerably slowed by the stellar wind, and reaches its maximum approach before reaching the *x*-axis, which is where the stagnation point should be according to the analytical model.

The departures from the analytical predictions seen in models M5 and M6 are not surprising. The model considers that the jet adopts the plasmon configuration derived from the plane parallel model (Cantó & Raga 1995). Therefore, the model is only valid when the scale-length of the jet cross section is small compared with the radius of curvature of the path.

5. H α emission

In this section, we present Hα emission maps computed assuming that the *xy*-plane of the simulations (which includes the O star and the outflow axis) is parallel to the plane of the sky. The results obtained from models M1-M6 (for the same time-frames as Fig. 3) are shown in Fig. 4.

The time-independent ejection velocity models (models M1, M2, M4 and M5, see 1 and Fig. 4) show a more or less continuous emission from the body of the curved jet beam. This emission is a result of the fact that the jet beam is fully photoionized.

The time-dependent ejection velocity models (models M3 and M6, see Fig. 4), show strong Hα emission from the internal

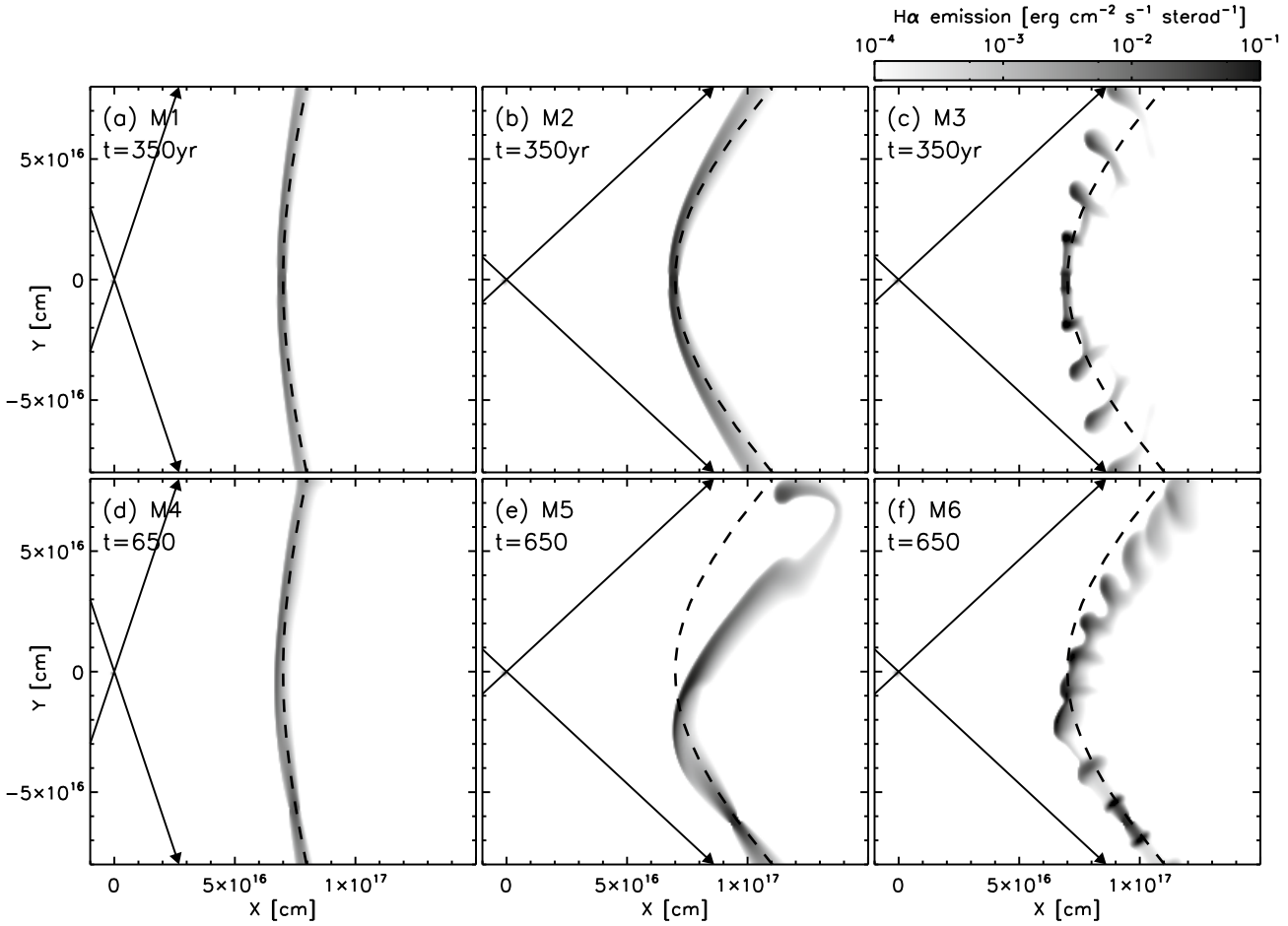

Fig. 4. H α maps for all the models. The maps have been computed assuming that the observer is located in the $-z$-direction. The H α intensity in erg cm^{-2} s^{-1} sterad^{-1} is given by the gray-scale bar (colorbar in the online version) at the *top*, the model and integration time by the label at the *upper-left* corner of each frame.

working surfaces, and only very weak emission from the jet beam segments in between the working surfaces. The emission from the individual working surfaces shows a "tadpole"-like morphology, with the "head" towards the O star, and the "tail" cutting across the curved jet axis.

This remarkable morphology has not yet been observed in any HH object. Therefore, this represents a prediction of what is expected to be observed when chains of knots along jets embedded in an O star wind (e. g., the jets from the proplyds close to θ Ori) are detected.

6. X-ray emission

It is interesting to note that even though the models described above do not produce an appreciable amount of X-ray emission, for appropriate parameters an O-star wind/jet interaction can indeed produce a substantial X-ray luminosity $L_{\rm x}$. In order to demonstrate this, we derive a simple analytic model for computing $L_{\rm x}$.

We do this following the ideas of Raga et al. (2002), who derived an analytic model that predicts the X-ray luminosity from the head of a HH jet. Following these authors, we note that the X-ray luminosity is dominated by free-free emission, which has an emission rate (integrated over all frequencies):

$$\Lambda_{\rm ff} = 1.85 \times 10^{-27}\,{\rm erg\,cm^{-3}s^{-1}}\,T^{1/2}n^2\,, \tag{11}$$

where the temperature T and the number density n (of H ions or of free electrons) are in cgs units (see e.g., Osterbrock 1989).

We now assume that the X-ray emission from the bow shock formed by the O star wind impinging on the jet beam is dominated by the head of the bow shock. From the strong shock jump conditions, one finds that the gas in this region has a temperature

$$T \approx 1.5 \times 10^7\,{\rm K}\left(\frac{v_{\rm n}}{1000\,{\rm km\,s^{-1}}}\right)^2\,, \tag{12}$$

and a number density

$$n \approx 4 n_{\rm w}\,, \tag{13}$$

where $v_{\rm n}$ is the component of the wind velocity perpendicular to the xy-plane trajectory of the jet (see Fig. 1), and $n_{\rm w}$ is the number density of the wind at the appropriate position.

Finally, we estimate the emitting volume (for a length dl along the jet) as:

$${\rm d}V = 0.4\pi {r_{\rm j}}^2 {\rm d}l\,, \tag{14}$$

where $r_{\rm j}$ is the radius that the jet cross section presents to the impinging wind, and we have assumed that the bow shock standoff distance is $\approx 0.2 r_{\rm j}$.

We can then compute the X-ray luminosity as

$$L_{\rm x} = \int_{-\infty}^{\infty} 0.4\pi {r_{\rm j}}^2 \Lambda_{\rm ff} {\rm d}l\,. \tag{15}$$

This integral can be computed analytically if one assumes that the X-ray emission is spatially limited to a region close to the

stagnation point (see Fig. 1), so that we can neglect the curvature of the jet trajectory, and that r_j is position-independent. One can then combine Eqs. (11)–(14) with the continuity equation for a constant velocity wind, and carry out the integral analytically to obtain

$$L_x = 1.3\times10^{-5}L_\odot \times\left(\frac{r_j}{10^{15}\,\mathrm{cm}}\right)^2\left(\frac{10^{16}\,\mathrm{cm}}{R_s}\right)^3\left(\frac{\dot{M}_w}{10^{-6}\,M_\odot\,\mathrm{yr}^{-1}}\right)^2\left(\frac{10^3\,\mathrm{km\,s}^{-1}}{v_w}\right), \quad (16)$$

where R_s is the stagnation distance of the jet trajectory (see Sect. 2). Inserting the parameters of our models (see Table 1), we find that in all cases we have $L_x < 10^{-7}L_\odot$. Such a luminosity is 2–3 orders of magnitude too low to be detected with Chandra observations at typical distances to HH jets.

However, for stagnation distances $R_s \sim 5\times10^{15}$ cm (one order of magnitude lower than the ones of our simulations, see Sect. 3.2) Eq. (16) gives $L_x \approx 1.84\times10^{-4}L_\odot$. This luminosity is similar to the (reddening-corrected) $1.3\times10^{-4}L_\odot$ X-ray luminosity estimated from the Chandra observations of HH 2 Pravdo et al. (2001), so that the emission could clearly be detected for such an object at the distance of the Orion nebula.

7. Summary

We presented 3D numerical simulations of a bipolar HH jet interacting with an isotropic stellar wind from an O star. The results from our simulations can be summarized as follows :

- The jet/isotropic wind interaction leads to the formation of a plasmon-shaped jet cross section (see Fig. 2) and a curved trajectory (see Fig. 3) for the jet beam.
- Constant ejection velocity jet/counterjet systems closely follow the curved path predicted by the analytic model of Raga et al. (2009a) (see models M1, M2 and M4 in Fig. 3), except in cases in which the ejection direction lies close to the direction towards the O star (models M5 and M6 in Fig. 3).
- Jets with variable ejection velocity have internal working surfaces with straighter trajectories and inter-knot regions with more curved trajectories than equivalent steady jet models (M3 and M6 in Fig. 3).
- We have computed Hα emission maps which can be compared with observations of HH jets in the vicinity of O stars Fig. 4.
- The models predict a peculiar morphology of the individual working surfaces that are formed by a velocity variability, which remains to be observed in HH objects near massive stars.
- We have estimated the X-ray luminosity from a simple analytic model, the wind/jet interaction in our simulations would not produce a detectable X-ray luminosity. However, if the stagnation distance (i.e. point of closest approach between the jet/counterjet path and the O star) is on the order of ∼300 AU) such objects would produce X-ray luminosities as high as $\sim10^{-4}L_\odot$.

We should point out that the Hα emission obtained in our models is rather weak compared to the emission from the H II region near massive stars (near θ-Ori for instance), thus direct imaging of these jets is unlikely to reveal their extended morphologies. However, observations in nearby star formation regions might be possible if the jets can be separated from the H II region in velocity, using for instance Fabry-Pérot interferometry.

Interestingly, a number of the Orion proplyds have been detected in X-rays. Kastner et al. (2005) report (deredened) X-ray luminosities in the $10^{-3} \rightarrow 10^{-5}$ range for ∼100 proplyds. For example, the LV2 (167-317) proplyd (one of the proplyds which are probably embedded in the wind from θ^1-Ori, see Sect. 1) has an X-ray luminosity of $\approx6.5\times10^{-4}\ L_\odot$. A fraction of this X-ray luminosity might be the result of the interaction between the jets associated with this object and the wind from θ^1 Ori C.

Acknowledgements. This work was supported by the DGAPA (UNAM) grant IN108207, the CONACyT grants 46828-F and 61547, and by the "Macroproyecto de Tecnologías para la Universidad de la Información y la Computación" (Secretaría de Desarrollo Institucional de la UNAM). We thank Enrique Palacios, Martín Cruz and Antonio Ramírez for their support of the servers in which the simulations were carried out.

References

Bally, J., & Reipurth, B. 2001, ApJ, 546, 299
Bally, J., O'Dell, C. R., & McCaughrean, M. J. 2000, AJ, 119, 2919
Bally, J., Licht, D., Smith, N., et al. 2006, AJ, 131, 473
Cantó, J., & Raga, A. C. 1995, MNRAS, 277, 1120
Ciardi, A., Ampleford, D. J., Lebedev, S. V., et al. 2008, ApJ, 678, 968
Kajdič, P., & Raga, A. C. 2007, ApJ, 670, 1173
Kastner, J. H., Franz, G., Grosso, N., et al. 2005, ApJS, 160, 511
Lim, A. J., & Raga, A. C. 1998, MNRAS, 298, 871
Masciadri, E., & Raga, A. C. 2001, AJ, 121, 408
Osterbrock, D. E. 1989, Astrophysics of gaseous nebulae and active galactic nuclei (Mill Valley: University Science Books)
Pravdo, S. H., Feigelson, E. D., Garmire, G., et al. 2001, Nature, 413, 708
Raga, A. C., Noriega-Crespo, A., & Velázquez, P. F. 2002, ApJ, 576, L149
Raga, A. C., Cantó, J., Rodríguez-González, A., & Esquivel, A. 2009a, A&A, 493, 115
Raga, A. C., Henney, W., Vasconcelos, J., et al. 2009b, MNRAS, 392, 964
Toro, E. F., Spruce, M., & Speares, W. 1994, Shock Waves, 4, 25